International Journal of Mechanical Engineering and Applications
2016; 4(1): 1-10
Published online January 21, 2016 (http://www.sciencepublishinggroup.com/j/ijmea)
doi: 10.11648/j.ijmea.20160401.11
ISSN: 2330-023X (Print); ISSN: 2330-0248 (Online)

Adaptive Tracking Control of a PMSM-Toggle System with a Clamping Effect

Yi-Lung Hsu, Ming-Shyan Huang, Rong-Fong Fung*

Department of Mechanical & Automation Engineering, National Kaohsiung First University of Science and Technology, Kaohsiung, Taiwan

Email address:
u9615907@nkfust.edu.tw (Yi-Lung Hsu), rffung@nkfust.edu.tw (Rong-Fong Fung)

To cite this article:
Yi-Lung Hsu, Ming-Shyan Huang, Rong-Fong Fung. Adaptive Tracking Control of a PMSM-Toggle System with a Clamping Effect. *International Journal of Mechanical Engineering and Applications.* Vol. 4, No. 1, 2016, pp. 1-10. doi: 10.11648/j.ijmea.20160401.11

Abstract: This paper discusses an adaptive control (AC) designed to track an energy-saving point-to-point (ESPTP) trajectory for a mechatronic system, which is a toggle mechanism driven by a permanent magnet synchronous motor (PMSM) with a clamping unit. To generate the PTP trajectory, we employed an adaptive real-coded genetic algorithm (ARGA) to search for the energy-saving trajectory for a PMSM-toggle system with a clamping effect. In this study, a high-degree polynomial was used, and the initial and final conditions were taken as the constraints for the trajectory. In the ARGA, the parameters of the polynomials were determined by satisfying the desired fitness function of the input energy. The proposed AC was established by the Lyapunov stability theory in the presence of a mechatronic system with uncertainties and the impact force not being exactly known. The trajectory was tracked by the AC in experimental results so as to be compared with results produced by trapezoidal and high-degree polynomials during motion.

Keywords: Adaptive Control, ARGA, Clamping Effect, Energy-Saving, Trajectory Planning

1. Introduction

This paper discusses adaptive control (AC) designed to track an energy-saving point-to-point (ESPTP) trajectory for a PMSM-toggle system. In general, this example is referred to as point-to-point control, and it takes into account low acceleration and jerk-free motion [1]. Astrom and Wittenmark [2] presented a general methodology for the off-line tridimensional optimal trajectory planning of robot manipulators in the presence of moving obstacles. Planning robot trajectory by using energetic criteria provides several advantages. On one hand, it yields smooth trajectories and is easy to track, while reducing the stress in the actuators and manipulator structures. Moreover, the minimum amount of energy may be desirable in several applications, such as those with energy-saving control or a quantitatively limited energy source [3]. Examples of minimum-energy trajectory planning are provided in [4]. However, the selection of a suitable profile for a specific application is still a challenge since it affects overall servo performance. Thus, in this study, the authors designed the kinematics of the trajectory profiles for motion tracking control within a PTP trajectory.

The AC techniques proposed in this study are essential to providing stable, robust performance for a wide range of applications such as robot control [5-9] and process control [10]. Most such applications are inherently nonlinear. Moreover, a relatively small number of general theories exist for the AC of nonlinear systems [11]. Since the application of a mechatronic system has minimum-energy tracking control problems for elevator systems, the AC technique developed by Chen [12], who made use of conservation of energy formulation to design control laws for the fixed position control problem, was adopted to control the PMSM-toggle system in this study. In addition, an inertia-related Lyapunov function containing a quadratic form of a linear combination of position- and speed-error states was formulated.

The difference between previous studies [13-18] and this study is that this study takes the clamping unit into consideration. The main contribution of this study is that the proposed AC adapts not only to parametric uncertainties of mass variations, but also to external disturbances. The performance with external disturbances is validated through the results obtained both numerically and experimentally on the energy-saving point-to-point trajectory processes for a PMSM-toggle system with a clamping unit.

2. Modeling of the Mechatronic System

2.1. Electrical Model

The permanent magnet synchronous motor drive toggle system is shown in Fig. 1, and the electromagnetic torque developed by the PMSM is

$$\tau_e = K_t i_q, \tag{1}$$

where τ_e is the electromagnetic torque, i_q is the current, and K_t is the motor torque constant. Usually, the PMSM is controlled by voltage command v_q^*. The machine model of a PMSM can be described as a rotating rotor coordinate. The electrical equation is

$$L_q \dot{i}_q + R_s i_q + \omega_s \lambda_d = v_q^*, \tag{2}$$

where L_q is the inductance, $\dot{i}_q$ is di_q / dt, R_s is the stator resistance, and ω_s and λ_d are the inverter frequency and stator flux linkages, respectively.

The applied torque can be obtained as follows:

$$\tau = n\left(\tau_e - J_m \dot{\omega}_r - B_m \omega_r\right), \tag{3}$$

where τ_e is the electromagnetic torque, the variables ω_r and $\dot{\omega}_r$ are the angular speed and acceleration of the rotor, respectively, B_m is the damping coefficient, and J_m is the moment of inertia. It is noted that $\omega_s = p\omega_r$, where p is the number of pole pairs and n is the ratio of the geared speed-reducer. Eqs. (2) and (3) represent the mathematical model of the PMSM. They give the voltage and motor torque variation with respect to time.

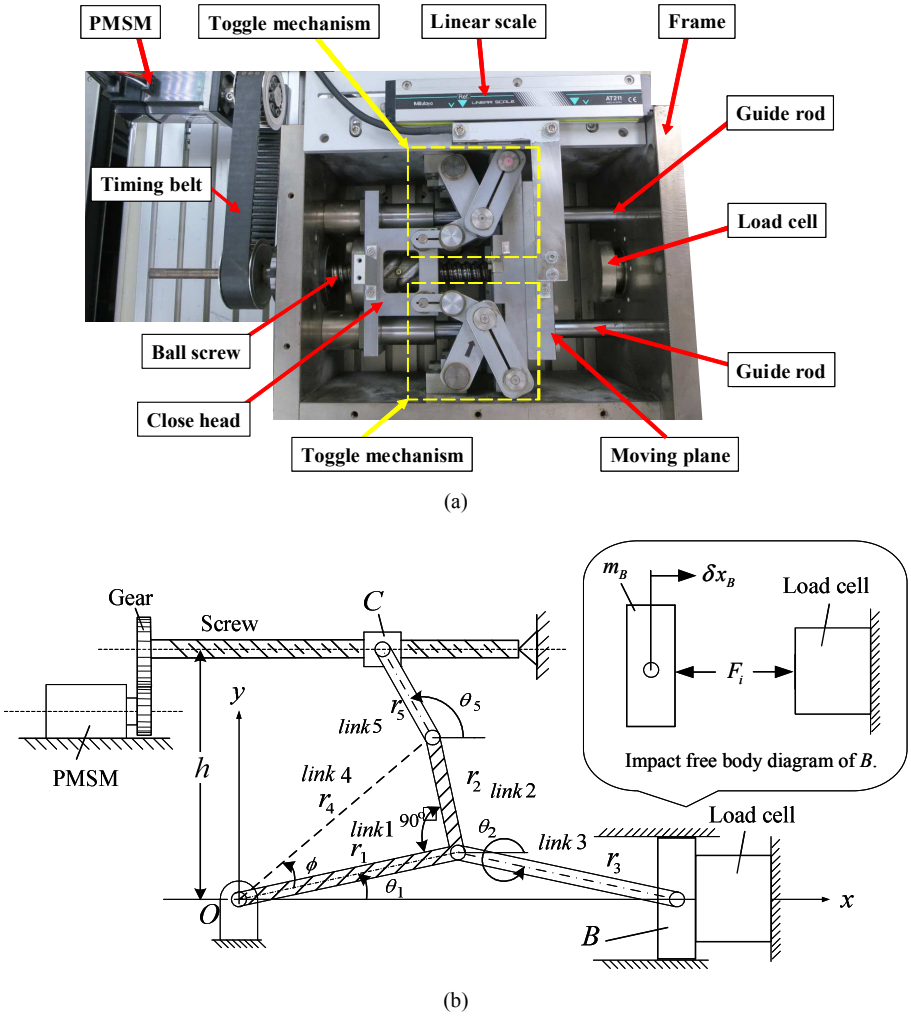

Fig. 1. *PMSM-toggle system with a clamping unit. (a) Photograph of experimental device. (b) Physical model.*

2.2. Impact Model

In this section, we consider the motion in a given stroke of the toggle mechanism undergoing impact when two objects collide over a very short period of time. The continuous force model approach [19] employs a logical spring-damper element to estimate the impact force between the two masses of the mechatronic system as,

$$F_i = K_l\, z + D_l \dot{z}, \tag{4}$$

where K_l is the elastic spring coefficient, z is the relative displacement or penetration between the surfaces of the two colliding bodies, $\dot{z}$ is the relative speed, and D_l is the damping coefficient. For the time period of $t_i^- \le t \le t_i^+$, the differential-algebraic equation can also be rewritten in matrix form. The impact model of the toggle mechanism with a clamping unit is shown in Fig. 2.

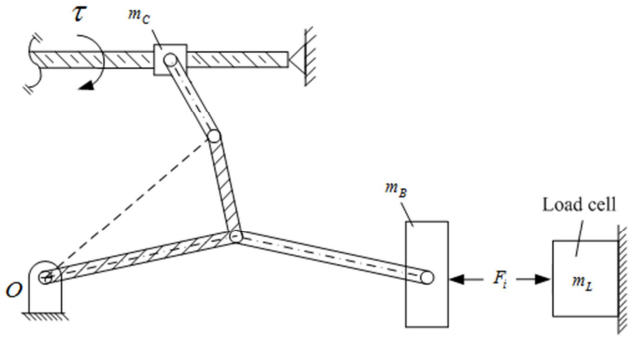

Fig. 2. *Impact model of toggle mechanism with a clamping unit.*

2.3. Mathematical Model of the Toggle Mechanism

The toggle mechanism of the electrical injection molding machine was driven by a PMSM. The experimental setup and physical model are shown in Fig. 1(a) and Fig. 1(b), respectively. The differential-algebraic equations of the toggle mechanism are summarized in matrix form [20]. The matrix form of the equations can be written as:

$$\hat{M}(\mathrm{v})\ddot{\mathrm{v}} + \hat{N}(\mathrm{v},\dot{\mathrm{v}}) = \hat{Q}(\mathrm{v})U + \hat{D}(\mathrm{v}). \tag{5}$$

where

$$\hat{M} = M^{vv} - \mathbf{M}^{vu}\boldsymbol{\Phi}_u^{-1}\boldsymbol{\Phi}_v - \boldsymbol{\Phi}_v^{\mathbf{T}}\left(\boldsymbol{\Phi}_u^{-1}\right)^{\mathbf{T}}\left[\mathbf{M}^{uv} - \mathbf{M}^{uu}\boldsymbol{\Phi}_u^{-1}\boldsymbol{\Phi}_v\right],$$

$$\hat{N} = \left[N^v - \boldsymbol{\Phi}_v^{\mathbf{T}}\left(\boldsymbol{\Phi}_u^{-1}\right)^{\mathbf{T}}\mathbf{N}^u\right] + \left[\mathbf{M}^{vu}\boldsymbol{\Phi}_u^{-1} - \boldsymbol{\Phi}_v^{\mathbf{T}}\left(\boldsymbol{\Phi}_u^{-1}\right)^{\mathbf{T}}\mathbf{M}^{uu}\boldsymbol{\Phi}_u^{-1}\right]\gamma,$$

$$\hat{Q} = B^v - \boldsymbol{\Phi}_v^{\mathbf{T}}\left(\boldsymbol{\Phi}_u^{-1}\right)^{\mathbf{T}}\mathbf{B}^u,\ U = i_q,$$

$$\hat{D} = D^v - \boldsymbol{\Phi}_v^{T}\left(\boldsymbol{\Phi}_u^{-1}\right)^{T}\mathbf{D}^u.$$

The elements of the vectors $\mathbf{u}$, v and matrices $\boldsymbol{\Phi}_u$, $\boldsymbol{\Phi}_v$, $\mathbf{M}^{uu}$, $\mathbf{M}^{uv}$, $\mathbf{M}^{vu}$, M^{vv}, $\mathbf{N}^u$ and N^v are detailed in [20]. The system Eq. (5) is an initial value problem and can be integrated by using the fourth order Runge-Kutta method.

3. Energy-Saving Trajectory Planning

This section discusses how the AC was designed to track an ESPTP trajectory for a PMSM-toggle system. The degrees of the polynomial depended on the number of end-point conditions, which are desired for smoothness in the resulting motion. In the simplest case, the motion is defined during the initial time t_0 and final time T, and it satisfies the end-point conditions of position, velocity and acceleration at any time. From the mathematical point of view, the problem is then to find a function such that

$$\mathrm{v} = \mathrm{v}(t), \qquad t \in [t_0, T]. \tag{6}$$

This problem can be easily solved by considering the polynomial function

$$\mathrm{v}(t) = a_0 + a_1 t + a_2 t^2 + a_3 t^3 + \ldots + a_m t^m, \tag{7}$$

where each coefficient a_i, $i = 0,\ldots,m$, is a real number, and a_m is a non-negative real number. The $m+1$ coefficients a_i, $i = 0,\ldots,m$, were determined such that the end-point constraints were satisfied. A high-degree polynomial was used to describe the trajectory, and it satisfied the desired constraints of position, velocity and acceleration at the end points.

For the PTP trajectory, we considered the profile with zero initial displacement, θ_1^h displacement at the final time T, a displacement and speed of 0 at t0, and $t = T$. Thus, we obtained the following end-point conditions:

$$\mathrm{v}(t_0) = 0,\ \dot{\mathrm{v}}(t_0) = 0, \tag{8}$$

$$\mathrm{v}(T) = \theta_1^h,\ \dot{\mathrm{v}}(T) = 0. \tag{9}$$

By using these four conditions and substituting them into equation (9) when $n = 12$, we obtain:

$$a_2 = \frac{3\theta_1^h}{T^2} + a_4 T^2 + 2a_5 T^3 + 3a_6 T^4 + 4a_7 T^5 + 5a_8 T^6 + 6a_9 T^7 + 7a_{10} T^8 + 8a_{11} T^9 + 9a_{12} T^{10}, \tag{10}$$

$$a_3 = \frac{-2\theta_1^h}{T^3} - 2a_4 T - 3a_5 T^2 - 4a_6 T^3 - 5a_7 T^4 - 6a_8 T^5 - 7a_9 T^6 - 8a_{10} T^7 - 9a_{11} T^8 - 10a_{12} T^9. \tag{11}$$

It is seen from Eqs. (10) and (11) that the two coefficients a_2 and a_3 can be obtained if the nine coefficients ($a_4 \sim a_{12}$) are known. In our trajectory design, the nine coefficients ($a_4 \sim a_{12}$) were determined by the adaptive real-coded

genetic algorithm (ARGA) method with an energy-saving fitness function.

The PMSM is considered thermodynamically as an energy converter. It takes electrical energy from a controlled input and then outputs it as mechanical work to drive the toggle mechanism system with a clamping unit. The input absolute electrical energy (IAEE) to the system is defined as

$$E_i = \int_0^T \left| i_q v_q \right| dt \tag{12}$$

where i_q is the electric current and v_q is the voltage command.

4. Adaptive Real-Coded Genetic Algorithm

It is important that crossover probability and mutation probability are set correctly for the genetic algorithms; improper settings will cause algorithms to only find local optimums and will also cause premature convergence. Therefore, an efficient method that allows for fast settings is essential. To resolve this, a mechanism to adjust the crossover probability and mutation probability according to the algorithmic performance was considered. In this study, the adaptive real-coded genetic algorithm for polynomial coefficient identification of the ESPTP trajectory of the PMSM-toggle system was employed.

In equations (10) and (11), there were nine unknown coefficients $a_4 \sim a_{12}$ to be determined by the ARGA. First, we defined the decision vector as

$$\mathbf{z} = \left[a_4, a_5, a_6, a_7, a_8, a_9, a_{10}, a_{11}, a_{12} \right]. \tag{13}$$

The procedure carried out for the ARGA is shown in Fig. 3. In this study, the procedure was reproduced through roulette wheel selection, while the crossover and uniform mutation were carried out through the methods described in [21].

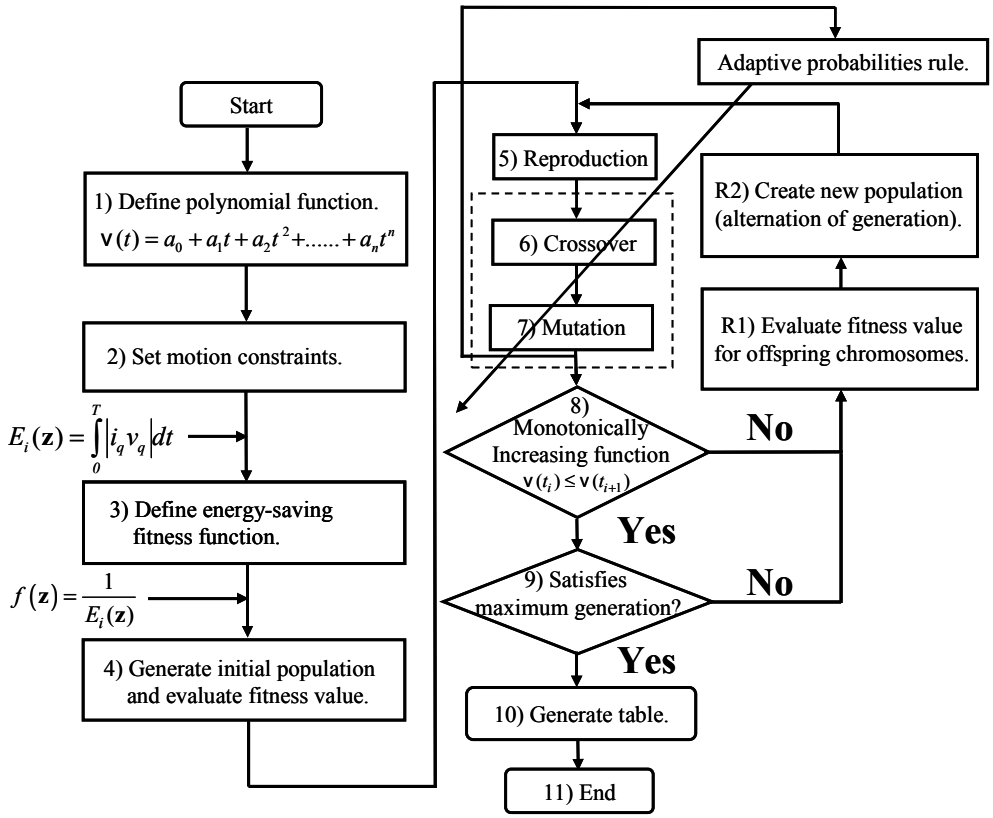

Fig. 3. *Flow chart for carrying out adaptive real-coded genetic algorithm.*

4.1. Fitness Function

How the fitness function is defined is the key to the genetic algorithm since the fitness function is a figure of merit and could be computed by using any domain knowledge. In the proposed ESPTP trajectory planning problem, the researchers defined the input energy function as the fitness function $f(\mathbf{z})$ as

$$f(\mathbf{z}) = \sum_{i=1}^{m} E_i(\mathbf{z}), \tag{14}$$

where m is the total number of samples and $E_i(\mathbf{z})$ is the input energy of the i^{th} sampling time.

4.2. Adaptive Probability Law

To reduce premature convergence and improve the convergence rate of the traditional real-coded genetic algorithm (TRGA), the adaptive probabilities of crossover and mutation were used in the ARGA. "Crossover" is the breeding of two parents to produce a single offspring which possesses features of both parents and thus may turn out better or worse than either parent according to the objective function. The primary purpose of mutation is to introduce variation, help bring back certain essential genetic traits, and avoid premature convergence of the entire feasible space caused by certain super chromosomes.

To reduce premature convergence and improve the convergence rate of the TRGA, the adaptive probabilities rule [21] of crossover and mutation were used in the ARGA. The probabilities of crossover Γ_c and mutation Γ_m are respectively given as follows:

$$\Gamma_c = \Gamma_c^{'} \times \left(1 + \alpha \frac{\left(F_{\text{avg}}\right)^{\delta_c}}{\left(F_{\max} - F_{\min}\right)^{\delta_c} + \left(F_{\text{avg}}\right)^{\delta_c}} \right), \tag{15}$$

$$\Gamma_m = \Gamma_m^{'} \times \left(1 + \beta \frac{\left(F_{\text{avg}}\right)^{\delta_c}}{\left(F_{\max} - F_{\min}\right)^{\delta_c} + \left(F_{\text{avg}}\right)^{\delta_c}} \right), \tag{16}$$

where $F_{\max}$, $F_{\min}$ and F_{avg} are the maximum, minimum and average individual fitness values of (14), respectively, $\Gamma_c^{'}$ and $\Gamma_m^{'}$ are the crossover and mutation probabilities, respectively, and α, β, and δ_c are coefficient factors. In this study, the values $\alpha = 0.24$, $\beta = 0.17$, and $\delta_c = 0.22$ [21] were used. From Eqs. (15) and (16), it can be seen that the adaptive Γ_c and Γ_m vary with fitness functions. Γ_c and Γ_m increase when the population tends to get stuck at a local optimum (when attraction basins are found around locally optimal points) and decrease when the population is scattered in the solution space.

4.3. Increasing Function

For the sake of tracking the motion profile of the mechatronic system, the trajectory displacement needs to be designed as a monotonically increasing function from the start point to the end point. In this study, $\mathrm{v}(t)$, $0 \le t \le T$ was assumed as the monotonically increasing function:

$$\mathrm{v}(t_i) \le \mathrm{v}(t_{i+1}), \quad t_i \le t_{i+1}, \tag{17}$$

where the subscript i represents the ith sampling time. This constraint of the monotonically increasing function had to be included in the procedure of the ARGA as shown in Fig. 3.

5. Adaptive Control Design

In this study, the researchers used the law of AC to describe what happens when two objects collide. "To adapt" means to change a behavior to conform to new circumstances. The AC law can control the two objects and balance the speed. The AC system is shown in Fig. 4, where x_B^* and x_B are the slider command position and slider position of the PMSM-toggle system, respectively. The slider position x_B is the desired control objective and can be manipulated by the relation $x_B = 2r_1 \cos\theta_1$, where the angle $\theta_1 = \mathrm{v}$ is the experimentally measured state as found by use of a linear encoder system.

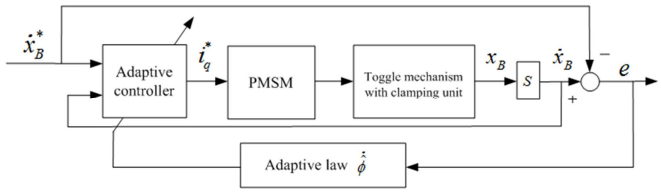

Fig. 4. *Block diagram of the AC system.*

In order to design an AC, the researchers rewrote Eq. (5) as a second-order nonlinear equation:

$$u(t) = f\left(\mathrm{v};t\right)\ddot{\mathrm{v}}\left(t\right) + G\left(\mathrm{v};t\right) - d\left(t\right), \tag{18}$$

where

$$f\left(\mathrm{v};t\right) = \hat{Q}^{-1}\hat{M}, \quad G\left(\mathrm{v};t\right) = \hat{Q}^{-1}\hat{N}, \quad d\left(t\right) = \hat{Q}^{-1}\hat{D},$$

and $u(t)$ is the control input voltage. It was assumed that the exact mass of slider B and the exact impact force F_i could not be known. With these uncertainties, the first step in designing the AC was to select a Lyapunov function, which is a function used for tracking error and parameter error. An inertia-related Lyapunov function containing a quadratic form of a linear combination of position- and speed-error states was chosen as follows [15]:

$$V = \frac{1}{2}s^T f(\mathrm{v};t)s + \frac{1}{2}\tilde{\phi}^T \Gamma^{-1}\tilde{\phi}, \tag{19}$$

where

$$s = \lambda_e e + \dot{e}, \quad e = \mathrm{v} - \mathrm{v}^*,$$

$$\Upsilon = \begin{bmatrix} \gamma_1 & 0 \\ 0 & \gamma_2 \end{bmatrix}, \ \tilde{\phi} = \phi - \hat{\phi}, \ \phi = \begin{bmatrix} m_B & F_i \end{bmatrix}^T, \ \hat{\phi} = \begin{bmatrix} \hat{m}_B & \hat{F}_i \end{bmatrix}^T.$$

and in which λ_e, γ_1 and γ_2 are positive scalar constants. The auxiliary signal s may be considered as a filtered tracking error.

Differentiating Eq. (19) with respect to time gives

$$\dot{V} = s^T f(\mathrm{v};t)\dot{s} + \frac{1}{2}s^T \dot{\hat{Q}}^{-1}\hat{M}s + \frac{1}{2}s^T \hat{Q}^{-1}\dot{\hat{M}}s + \tilde{\phi}^T \Upsilon^{-1}\dot{\tilde{\phi}}, \quad (20)$$

and by multiplying the variable $\dot{s}$ with Eq. (20), we obtain

$$f(\mathrm{v};t)\dot{s} = f(\mathrm{v};t)(\lambda_e \dot{e} - \ddot{x}_B^* + \ddot{x}_B) = A(\bullet) + B(\bullet)\phi - 2\eta \sin\theta_1 u, \quad (21)$$

where $A(\bullet)$ and $B(\bullet)$ are described in reference [15]. Substituting Eq. (21) into Eq. (20) gives

$$\begin{aligned}\dot{V} &= s^T\left[A(\bullet) + B(\bullet)\phi - 2\eta \sin\theta_1 u\right] + \frac{1}{2}s^T \dot{\hat{Q}}^{-1}\hat{M}s + \frac{1}{2}s^T \hat{Q}^{-1}\dot{\hat{M}}s + \tilde{\phi}^T \Upsilon^{-1}\dot{\tilde{\phi}} \\ &= s^T\left[A'(\bullet) + B'(\bullet)\phi - 2\eta \sin\theta_1 u\right] + \tilde{\phi}^T \Upsilon^{-1}\dot{\tilde{\phi}},\end{aligned} \quad (22)$$

where $A'(\bullet)$ and $B'(\bullet)$ are described in reference [15]. If the control input is selected as

$$u = \frac{\left[A'(\bullet) + B'(\bullet)\hat{\phi} + K_V s\right]}{2\eta \sin\theta_1}, \quad (23)$$

where K_V is a positive constant, then Eq. (22) becomes

$$\dot{V} = -s^T K_V s + \tilde{\phi}^T\left[\Upsilon^{-1}\dot{\tilde{\phi}} + B'(\bullet)^T s\right]. \quad (24)$$

By selecting the adaptive update rule as

$$\dot{\tilde{\phi}} = -\dot{\hat{\phi}} = -\Upsilon B'(\bullet)^T s, \quad (25)$$

and substituting it into Eq. (24), it then becomes

$$\dot{V} = -s^T K_V s \le 0. \quad (26)$$

Since $\dot{V}$ in Eq. (26) is negative semi-definite, then V in Eq. (19) is upper-bounded. As V is upper-bounded and $f(\mathrm{v};t)$ is a positive-definite matrix, it can be said that s and $\tilde{\phi}$ are bounded.

6. Numerical Simulations and Experiment Results

6.1. Numerical Simulations

This section discusses how the researchers simulated the ESPTP motion profile for the PMSM-toggle system. The trajectory profile $\mathrm{v}(t)$ was chosen as a monotonically increasing function. The input absolute electrical energy E_i was calculated by the fourth-order Runge-Kutta method via a Windows supported MATLAB package with a sampling time of $\Delta t = 0.01$ sec and the time interval being from 0 to 1 sec. In the numerical simulations, we adopted the parameters of the PMSM-toggle system obtained as follows:

$m_2 = 1.82$ (kg), $m_3 = 1.61$ (kg), $m_5 = 0.95$ (kg), $m_B = 8.86$ (kg), $m_C = 5.58$ (kg),
$r_1 = 0.06$ (m), $r_2 = 0.032$ (m), $r_3 = 0.06$ (m), $r_4 = 0.068$ (m), $r_5 = 0.03$ (m), $l_d = 0.01$ (m),
$h = 0.068$ (m), $K_t = 0.565$ (Nm/A), $J_m = 6.72\times10^{-5}$ (Nms^2), $B_m = 1.21\times10^{-2}$ (Nms/rad),
$K_l = 1.056\times10^7$ (kN/m), $D_l = 970$ (Ns/ m).

In the numerical simulations, the fitness value increased as the generation number increased, and almost all of the genes $(a_4, a_5, \cdots, a_{12})$ of the chromosome converged near the 30^{th} generation for the twelfth-degree polynomial as shown in Figs. 5(a)-5(d). Figures 5(a) and 5(b) show the displacements and speeds. From the comparisons in Fig. 5(c), it is demonstrated that the ARGA is more efficient in identifying polynomial coefficients than the TRGA. The energy used was less than 9×10^{-3} J. It is thus concluded that the ARGA does not only find local optimums while preventing premature convergence, the fitness values of the ARGA are greater than those of the TRGA.

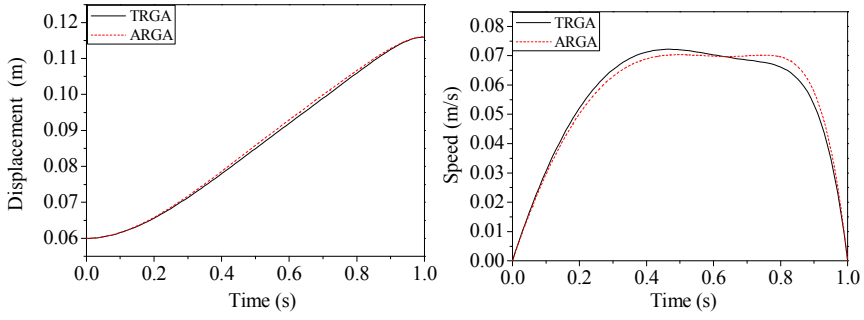

(a) (b)

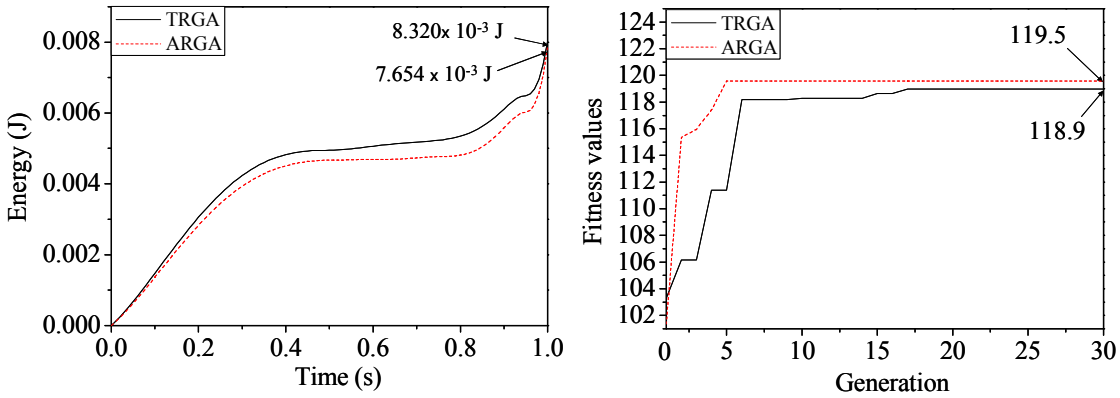

(c) (d)

Fig. 5. *Comparisons of the TRGA and ARGA for 12th-degree polynomials in numerical simulations. (a) Displacement. (b) Speed. (c) IAEE. (d) Fitness values.*

The comparisons of dynamic responses of the PMSM-toggle system for trapezoidal, fourth-degree, and twelfth-degree polynomials are shown in Figs. 7(a)-7(d). The speeds are compared in Fig. 7(c). The displacement- and speed-error comparisons with respect to the trapezoidal, fourth-degree and twelfth-degree polynomials are shown in Figs. 7(b) and 7(d). (The fourth-degree and twelfth-degree polynomials were formulated based on ESPTP trajectories.) The final identification of the polynomial coefficients a4 ~ a12, the values of the fitness function of the mechatronic system, and the highest fitness value were found by using the twelfth-degree polynomial. The total energy values are also compared in Table 1, where the final values are about 8.320×10^{-3}J , 9.661×10^{-3}J, and 7.654×10^{-3}J. The lowest value is that of the twelfth-degree polynomial, and the trapezoidal polynomial had a relative reduction of -8% in input energy.

6.2. Experimental Setup

A photo of the PMSM-toggle system with a clamping unit is shown in Fig. 1(a), and the experimental equipment used is shown in Fig. 6. The control algorithm was implemented by using a Celeron computer, and the control software used was LabVIEW. The PMSM was driven by a Mitsubishi HC-KFS13 series. The specifications were set as follows: rated torque of 1.3 Nm, rated rotation speed of 3k rpm, rated output of 0.1 kW, and rated current of 0.7 A. The servo-motor was driven by a Mitsubishi MR-J2S-10A.

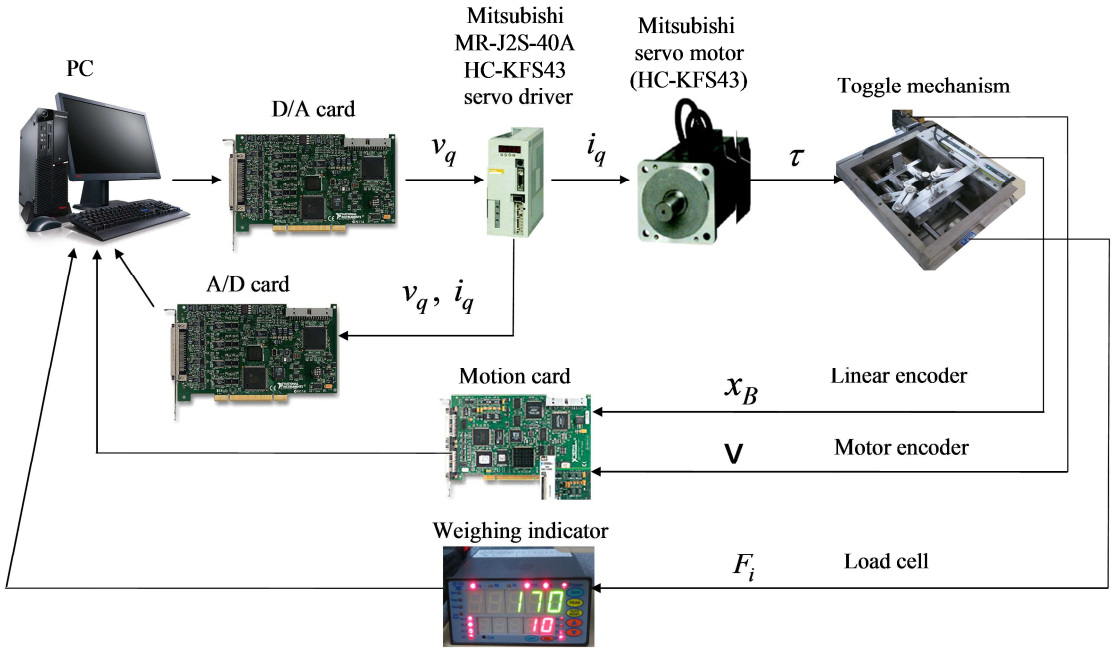

Fig. 6. *Experimental equipment for the PMSM-toggle system with a clamping unit.*

6.3. Experimentation

For the ESPTP trajectory processes of a PMSM-toggle system, the control objective was to control the position of slider *B* to move from the start-position of 0 m to the end-position of 0.116 m with the clamping point at 0.1159 m. The numerical simulations and experimental results of

trapezoidal, fourth-degree and twelfth-degree polynomials for the ESPTP trajectory displacement and speed tracking control by the AC are shown in Figs. 7(a)-7(h). The control gains are $\lambda_e = 0.5$, γ_1=104, γ_2=209, K_V=6. Figures 7(a) and 7(b) show the displacement, and their tracking error is less than about -0.5 mm of the ESPTP trajectory of the numerical simulations and experimental results. Figures 7(c) and 7(d) show the speed of the PMSM-toggle system, and their errors are slight. Moreover, the command input, input current, impact force and input energy with the clamping effect are shown in Figs. 7(e)-7(h). As seen from the experimental results, accurate tracking control performance of the PMSM-toggle system with a clamping unit can be obtained after the clamping point of the ESPTP trajectory of the AC system, and adaptive characteristics were achieved for the AC system. The final input energy values were about 79.9 J, 99.4 J and 51.1 J, respectively. The total energy comparisons are shown in Table 1. The lowest value is that of the twelfth-degree polynomial, and the trapezoidal polynomial had a relative reduction of -36% in input energy. In conclusion, the clamping time was shorter and the speed profile was smoother. Moreover, a better energy-saving effect can be achieved for a PTP trajectory with a clamping effect by using the AC system.

Table 1. *Comparisons of input energy for the numerical simulation and experimental trajectory planning of the trapezoidal, 4th-degree, and 12th-degree polynomials of the PMSM-toggle system.*

Trajectory planning of the trapezoidal, 4th-, and 12th-degree polynomials	**IAEE (J)**	
	Numerical simulation by ARGA without a clamping unit	**Experimental results by AC with a clamping unit**
Trapezoidal	8.320×10^{-3} J	79.9 J
4th-Degree	9.661×10^{-3} J	99.4 J
12th-Degree	7.654×10^{-3} J.	51.1 J

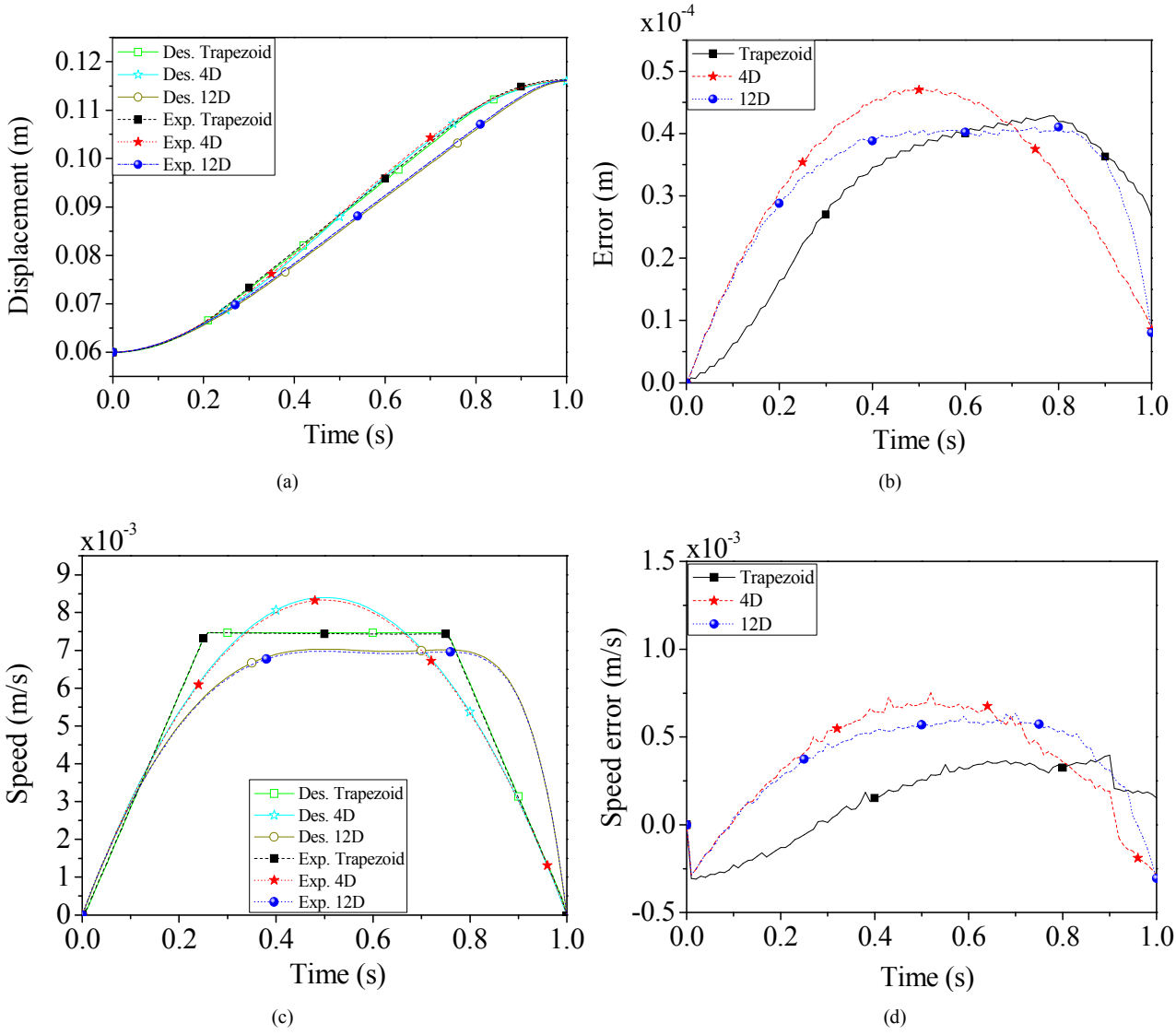

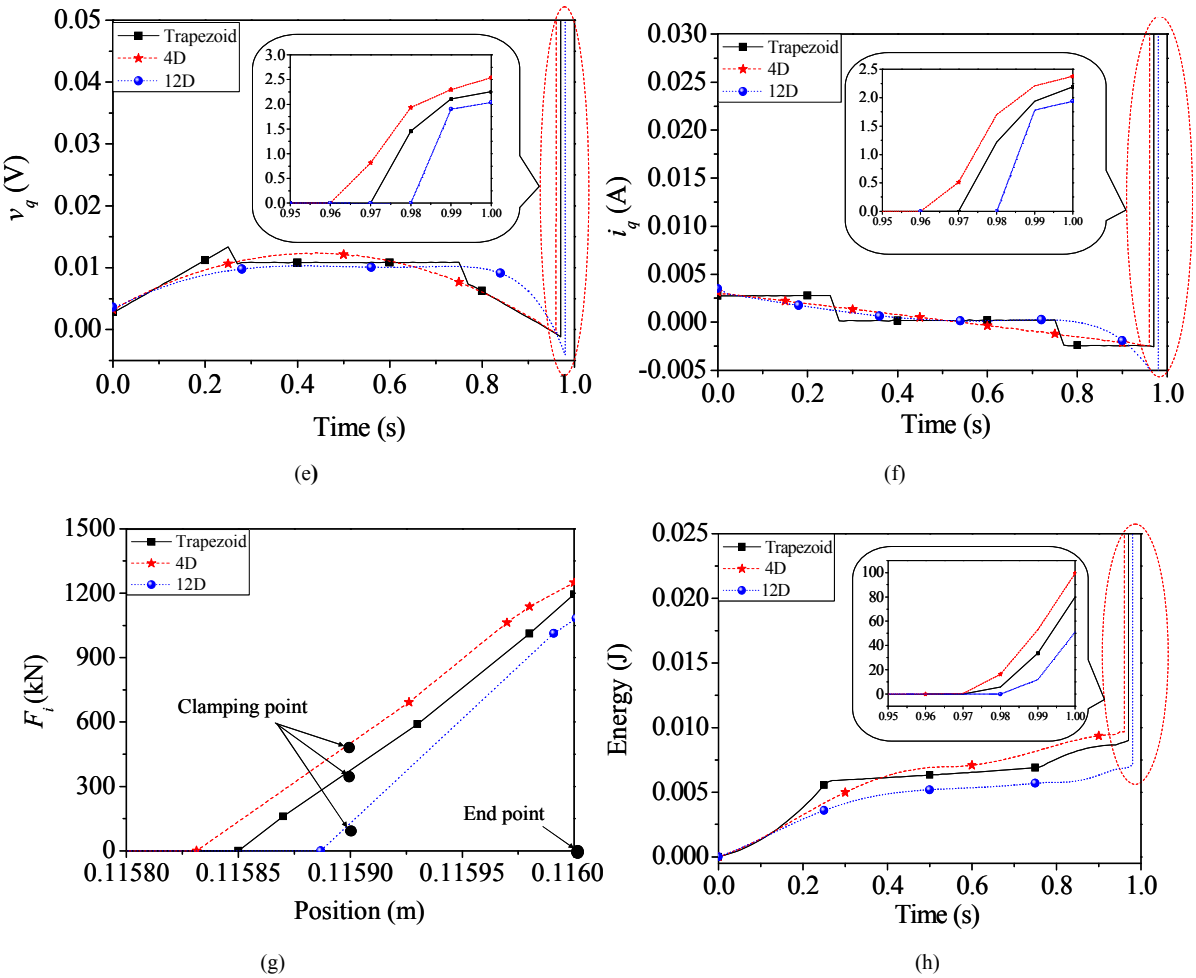

Fig. 7. *Comparisons of numerical simulations and experimental results for trapezoidal, fourth-degree and twelfth-degree polynomials by AC. (a) Displacement tracking. (b) Displacement tracking error. (c) Speed tracking. (d) Speed tracking error. (e) Input voltage. (f) Input current. (g) Impact force. (h) IAEE.*

7. Conclusion

A mathematical model was put into use for a PMSM-toggle system with a clamping unit, and the ESPTP trajectory for the mechatronic system was successfully planned by the adaptive real-coded genetic algorithm method described in this paper. The proposed AC was established by the Lyapunov stability theory for a mechatronic system with uncertainties and the impact force not being exactly known. The proposed methodology described in this paper was applied to a mechatronic system with a clamping unit. The mechatronic system required the design of an ESPTP trajectory which can be interpreted by any continuous function and which has different motion constraints at the start and end points. The results demonstrate that the adaptive control performance in the PTP trajectory with a clamping effect is successful for a mechatronic system.

Acknowledgement

The financial support from the Ministry of Science and Technology of the Republic of China with contract number MOST 103-2221-E-327 -009 -MY3 is gratefully acknowledged.

References

[1] Pu, J., Weston, R. H. and Moore, P. R., Digital Motion Control and Profile Planning for Pneumatic Servos, *ASME J. of DSMC*, Vol. 114, No. 4, pp. 634-640, 1992.

[2] Astrom, K. J. and Wittenmark, B., Adaptive Control, *Addison-Wesley, MA*, 1994.

[3] Slotine, J. J. E. and Li, W., Composite Adaptive Control of Robot Manipulators, *Automatica*, Vol. 25, No. 4, pp. 509-519, 1989.

[4] Biagiotti, L. and Melchiorri, C., Trajectory Planning for Automatic Machines and Robots, *Springer-Verlag*, 2008.

[5] Mohamed, Y. A. -R. I., Design and Implementation of a Robust Current-Control Scheme for a PMSM Vector Drive With a Simple Adaptive Disturbance Observer, *IEEE Trans. on Industrial Electronics*, Vol. 54, No. 4, pp. 1981-1988, 2007.

[6] Kim, K. H., Model Reference Adaptive Control-Based Adaptive Current Control Scheme of a PM Synchronous Motor with an Improved Servo Performance, *IET Electric Power Applications*, Vol. 3, No. 1, pp. 8-18, 2009.

[7] Shihua, L. and Zhigang, L., Adaptive Speed Control for Permanent-Magnet Synchronous Motor System with Variations of Load Inertia, *IEEE Trans. on Industrial Electronics*, Vol. 56, No. 8, pp. 3050-3059, 2009.

[8] Lee, D. H., Lee, J. H. and Ahn, J. W., Mechanical Vibration Reduction Control of Two-Mass Permanent Magnet Synchronous Motor Using Adaptive Notch Filter with Fast Fourier Transform Analysis, *IET Electric Power Applications*, Vol. 6, No. 7, pp. 455-461, 2012.

[9] Cho, S. H. and Helduser, S., Robust Motion Control of a Clamp-Cylinder for Energy-Saving Injection Moulding Machines, *Journal of Mechanical Science and Technology*, Vol. 22, No. 12, pp. 2445-2453, 2008.

[10] Kendra, S. J., Basila, M. R. and Cinar, A., Intelligent Process Control with Supervisory Knowledge-Based Systems, *IEEE Control Systems*, Vol. 14, No. 3, pp. 37-47, 1994.

[11] Wai, R. J., Adaptive Sliding-Mode Control for Induction Servomotor Drive, *IEE Proceedings on Electric Power Applications*, Vol. 147, No. 6, pp. 553-562, 2000.

[12] Chen, K. Y., Huang, M. S. and Fung, R. F., Adaptive Minimum-Energy Tracking Control for the Mechatronic Elevator System, *IEEE Trans. on Control Systems Technology*, Vol. PP, No. 99, 2013.

[13] Fung, R. F. and Chen, K. W., Dynamic Analysis and Vibration Control of a Flexible Slider-Crank Mechanism Using PM Synchronous Servo Motor Drive, *Journal of Sound and Vibration*, Vol. 214, No. 4, pp. 605-637, 1998.

[14] Lin, F. J., Fung, R. F. and Wai, R. J., Comparison of Sliding-Mode and Fuzzy Neural Network Control for Motor-Toggle Servomechanism, *IEEE/ASME Transactions on Mechatronics*, Vol. 3, No. 4, pp. 302-318, 1998.

[15] Chuang, C. W., Huang, M. S., Chen, K. Y. and Fung, R. F., Adaptive Vision-Based Control of a Motor-Toggle Mechanism: Simulations and Experiments, *Journal of Sound and Vibration*, Vol. 312, No. 4-5, pp. 848-861, 2008.

[16] Fung, R. F. and Chang, C. F., Force/Motion Sliding Mode Control of Three Typical Mechanisms, *Asian Journal of Control*, Vol. 11, No. 2, pp. 196-210, 2009.

[17] Cerman, O. and Hušek, P., Adaptive Fuzzy Sliding Mode Control for Electro-Hydraulic Servo Mechanism, *Expert Systems with Applications*, Vol. 39, No. 11, pp. 10269-10277, 2012.

[18] Cho, S. H. and Fung, R. F., Virtual Design of a Motor-Toggle Servomechanism with Sliding Mode-Combined PID Control, *Proceedings of the Institution of Mechanical Engineers, Part C: Journal of Mechanical Engineering Science*, pp. 1-10, 2014. DOI: 10.1177/0954406214531944

[19] Khulief, Y. A. and Shabana, A. A., A Continuous Force Model for the Impact Analysis of Flexible Multibody Systems, *Mechanism and Machine Theory*, Vol. 22, No. 3, pp. 213-224, 1987.

[20] Hsu, Y. L., Huang, M. S. and Fung, R. F., Convergent Analysis of an Energy-Saving Trajectory for a Motor-Toggle System, *Journal of Vibration Engineering and Technologies*, Vol. 3, No. 1, pp. 95-112, 2015.

[21] Du, Y., Fang, J. and Miao, C., Frequency-Domain System Identification of an Unmanned Helicopter Based on an Adaptive Genetic Algorithm, *IEEE Trans. on Industrial Electronics*, Vol. 61, No. 2, pp. 870-881, 2014.